Evolution of TLS with PDM under a Field Enhanced by a Spherical Nanoparticle

TSSP project under the supervision of Piotr Gładysz and Prof. Karolina Słowik

Niya Petkova

July - August 2023

Contents

1 Notation Guide

TLS: two-level system(s)
PDM: permanent dipole moment
$|g\rangle$: ground state of the TLS
$|e\rangle$: excited state of the TLS
e: elementary charge
$\vec{d} = e\vec{R}$: dipole moment with $\vec{R}$: position of particle
ω: frequency of the incident light
$\omega_0 = \omega_e - \omega_g$: frequency difference between the two atomic levels
$\delta = \omega_0 - \omega$: detuning
γ: spontaneous emission factor
$k = 2\frac{\pi}{\lambda}$: wavenumber (in vacuum)
E_0: amplitude of the incident electric field, which has the form:
$E = E_0 cos(\omega t)$. Light is assumed to have an $\hat{x}$ polarization and to travel in the $\hat{z}$ direction.
Ω_R: Rabi frequency. For a polar system: $\Omega_R = \frac{d_{eg}}{d_{ee}-d_{gg}}\omega J_1(\kappa)$
κ: contains dependence on incident field: $\kappa = \frac{E_0}{\hbar\omega}(d_{ee} - d_{gg})$
α: unknown constant introduced to solve the optical Bloch equations
$\Omega = \sqrt{\frac{\delta}{2}^2 + |\Omega_R|^2}$ for the detuning case
$J_n(x)$: Bessel function of the first kind of the nth order with argument x
$Y_n(x)$: Bessel function of the second kind of the nth order with argument x
$H_n^{(1)}(x)$: Hankel function of the first kind of the nth order with argument x
r, θ, ϕ: spherical coordinates
In the Mie scattering formalism, $\rho = kr$. Note that ρ also refers to the density matrix.
a: radius of spherical nanoparticle
$m = n + in'$: refractive index (of the nanoparticle material)

2 Introduction

The aim of this project is to find an analytical solution to the emission of TLS with PDM positioned at different points around an enhancing nanosphere. The Rabi frequency of oscillations between the $|g\rangle$ (ground) and $|e\rangle$ (excited) states of a TLS varies linearly with the intensity of incident light; however, when the system possesses a PDM, this relationship becomes parabolic (see Figure 1). Such atoms, if placed in the regime near the maximum of the curve, should be able to emit light in a coherent manner, at least over small timescales of the oscillation. A major drawback of this scheme is the requirement of high intensity fields. A nanosphere is proposed as a method to enhance the field strength at two hotspots where arrays of TLS can be positioned.

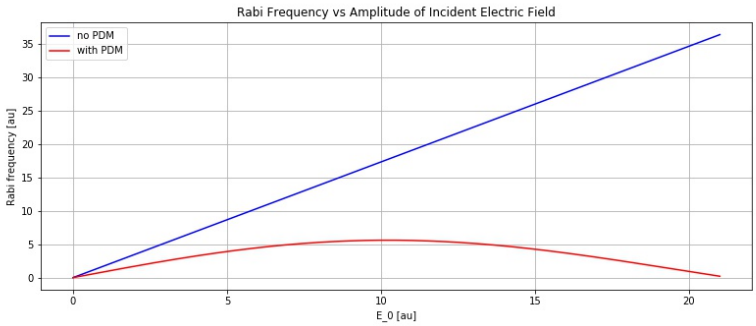

Figure 1: Rabi Frequency of Oscillations

3 Time Evolution of a TLS

This section follows the same method as outlined in [1]

The first step of the project is to derive the time evolution of the TLS based on the properties of the incident light. Because the intended field intensity is very strong, perturbation theory is not applicable. Luckily, in the case of a TLS, the problem has an analytical solution that can be obtained either via a direct tackling of the probability amplitudes of the two levels or by the density matrix method. Only the latter will be considered here, but over the course of the project both procedures were found to give the same results.

3.1 Hamiltonian

The Hamiltonian of a TLS under the influence of an electromagnetic field consists of an atomic term $\hat{H}_0$, inherent to the system, and an interaction term $\hat{H}_1$, describing the coupling to the external field. Assuming energies $\hbar w_g$, $\hbar w_e$ of the two levels, the atomic eigenvalue equations read

$$\hat{H}_0|g\rangle = \hbar w_g|g\rangle \tag{1}$$

$$\hat{H}_0|e\rangle = \hbar w_e|e\rangle \tag{2}$$

Using the identity operator $\hat{I} = |g\rangle\langle g| + |e\rangle\langle e|$ and the orthonormality of basis states:

$$\begin{aligned}
\hat{H}_0 &= \hat{I}\hat{H}_0\hat{I} && (3)\\
&= (|g\rangle\langle g| + |e\rangle\langle e|)\hat{H}_0(|g\rangle\langle g| + |e\rangle\langle e|) && (4)\\
&= (|g\rangle\langle g| + |e\rangle\langle e|)(\hbar w_g|g\rangle\langle g| + \hbar w_e|e\rangle\langle e|) && (5)\\
&= \hbar w_g|g\rangle\langle g| + \hbar w_e|e\rangle\langle e| && (6)
\end{aligned}$$

For systems of a size much smaller than the wavelength of the incident light that undergo fast optical transitions, an electric dipole approximation allows to neglect the effect of the magnetic field, as it is much smaller compared to the influence of the electric field. Assuming a field of the form $E = E_0 cos(\omega t)$, the potential energy of an electron with dipole moment $\vec{d}$ can then be described by a single term $\hat{V} = -\hat{\vec{d}} \cdot \vec{E_0} cos(\omega t)$, which forms the interaction Hamiltonian $\hat{H}_1$. Using the same approach as in Eq-ns (3):(6), this can be expressed in terms of the basis states as

$$\hat{H}_1 = \vec{E_0} cos(\omega t) \cdot (\vec{d_{gg}}|g\rangle\langle g| + \vec{d_{ge}}|g\rangle\langle e| + \vec{d_{eg}}|e\rangle\langle g| + \vec{d_{ee}}|e\rangle\langle e|) \tag{7}$$

where d_{ee}, d_{gg} define the permanent dipole moment of the system (zero for non-polar systems) and d_{ge}, d_{eg} describe the dipole moment induced by the external field (always non-zero).

The full Hamiltonian is the sum of the unperturbed and interaction Hamiltonians:

$$\begin{aligned}
\hat{H} &= \hat{H}_0 + \hat{H}_1 && (8)\\
&= (\hbar w_g - \vec{E_0} \cdot \vec{d_{gg}})|g\rangle\langle g| - \vec{E_0} cos(\omega t) \cdot (\vec{d_{ge}}|g\rangle\langle e| + \vec{d_{eg}}|e\rangle\langle g|) && (9)\\
&+ (\hbar w_e - \vec{E_0} \cdot \vec{d_{ee}})|e\rangle\langle e| && (10)
\end{aligned}$$

This has matrix elements

$$\begin{aligned}
H_{gg} &= \langle g|\hat{H}|g\rangle = \hbar w_g - \vec{E_0} \cdot \vec{d}_{gg} cos(\omega t) && (11)\\
H_{ge} &= \langle g|\hat{H}|e\rangle = \vec{E_0} \cdot \vec{d}_{ge} cos(\omega t) && (12)\\
H_{eg} &= \langle e|\hat{H}|g\rangle = \vec{E_0} \cdot \vec{d}_{eg} cos(\omega t) && (13)\\
H_{ee} &= \langle e|\hat{H}|e\rangle = \hbar w_e - \vec{E_0} \cdot \vec{d}_{ee} cos(\omega t) && (14)
\end{aligned}$$

so, finally, the Hamiltonian can be put into matrix form as

$$\underline{\underline{H}} = \begin{pmatrix} \hbar w_g - \vec{E_0} \cdot \vec{d}_{gg} cos(\omega t) & -\vec{E_0} \cdot \vec{d}_{ge} cos(\omega t) \\ -\vec{E_0} \cdot \vec{d}_{eg} cos(\omega t) & \hbar w_e - \vec{E_0} \cdot \vec{d}_{ee} cos(\omega t) \end{pmatrix} \tag{15}$$

Without loss of generality, the incident electric field is assumed for the remainer of the report to have an $\hat{x}$ polarization and to be travelling along the positive z-axis. Positioning the dipoles parallel to this field allows for the vector notation in (15) to be omitted.

3.2 The von Neumann Equation

Chapter 3 of reference [2] is a good introduction to density matrices

The Hamiltonian of the TLS can be used to solve the von Neumann equation for the time evolution of the system:

$$i\hbar\frac{\partial\hat{\rho}}{\partial t} = [\hat{H}, \hat{\rho}] \tag{16}$$

For a TLS, the density operator $\hat{\rho}$ is given in matrix form by

$$\underline{\underline{\rho}} = \begin{pmatrix} \rho_{gg} & \rho_{ge} \\ \rho eg & \rho_{ee} \end{pmatrix} \tag{17}$$

where $Tr(\underline{\underline{\rho}}) = \rho_{gg} + \rho_{ee} = 1$ follows from the normalisation condition, and the coherences are related by $\rho_{ge} = \rho^*_{eg}$. Therefore, it is only necessary to find two of the elements of the density matrix (for example, ρ_{ee} and ρ_{eg}, and the rest will follow from the properties of the density operator.

3.3 Optical Bloch Equations

Substituting (15) and (17) in the von Neumann equation (16) and following some simplifications, a relationship is obtained for the time derivatives of the density operator elements:

$$\dot{\rho}_{ee} = \frac{iE_0}{\hbar}cos(\omega t)(\rho_{ge}d_{eg} - \rho_{eg}d_{ge}) \tag{18}$$

$$\dot{\rho}_{eg} = -i(\omega_e - \omega_g)\rho_{eg} + \frac{iE_0}{\hbar}cos(\omega t)[\rho_{eg}(d_{ee} - d_{gg}) - d_{eg}(\rho_{ee} - \rho_{gg})] \tag{19}$$

$$\dot{\rho}_{ge} = i(\omega_e - \omega_g)\rho_{ge} - \frac{iE_0}{\hbar}cos(\omega t)[\rho_{ge}(d_{ee} - d_{gg}) - d_{ge}(\rho_{gg} - \rho_{ee})] \tag{20}$$

$$\dot{\rho}_{gg} = \frac{iE_0}{\hbar}cos(\omega t)(\rho_{eg}d_{ge} - \rho_{ge}d_{eg}) \tag{21}$$

$$\tag{22}$$

These four expressions known as the optical Bloch equations.

The following substitution with $\kappa = \frac{E_0}{\hbar\omega}(d_{ee} - d_{gg})$ can now be applied:

$$\rho_{eg} = \sigma_{eg}e^{-i\omega t}e^{i\kappa sin(\omega t)} \tag{23}$$

$$\dot{\rho}_{eg} = -i\omega\sigma_{eg}e^{-i\omega t}e^{i\kappa sin(\omega t)} + i\omega\kappa cos(\omega t)\sigma_{eg}e^{-i\omega t}e^{i\kappa sin(\omega t)} \tag{24}$$

$$+ \dot{\sigma}_{eg}e^{-i\omega t}e^{i\kappa sin(\omega t)} \tag{25}$$

Using the fact that the two coherences must be complex conjugates of each other and assuming there is no detuning ($\omega = \omega_e - \omega_g = \omega_0$), equations (18) -

(22) read

$$\dot{\rho}_{ee} = \frac{iE_0}{2\hbar}(e^{i\omega t} + e^{-i\omega t})(\sigma_{ge}d_{eg}e^{i\omega t}e^{-i\kappa sin(\omega t)} - \sigma_{eg}d_{ge}e^{-i\omega t}e^{i\kappa sin(\omega t)}) \quad (26)$$

$$\dot{\sigma}_{eg} = \frac{-iE_0}{2\hbar}d_{eg}(\rho_{ee} - \rho_{gg})(e^{2i\omega t} + 1)e^{-i\kappa sin(\omega t)} \quad (27)$$

$$\dot{\sigma}_{ge} = \frac{iE_0}{2\hbar}d_{ge}(\rho_{gg} - \rho_{ee})(e^{-2i\omega t} + 1)e^{i\kappa sin(\omega t)} \quad (28)$$

$$\dot{\rho}_{gg} = \frac{iE_0}{2\hbar}(e^{i\omega t} + e^{-i\omega t})(\sigma_{eg}d_{ge}e^{-i\omega t}e^{i\kappa sin(\omega t)} - \sigma_{ge}d_{eg}e^{i\omega t}e^{-i\kappa sin(\omega t)}) \quad (29)$$

But the exponential $e^{i\kappa sin(\omega t)}$ can be rewritten as $\sum_{n=-\infty}^{n=\infty} J_n(\kappa)e^{in\omega t}$ in terms of Bessel functions, so equations (26) - (29) become

$$\dot{\rho}_{ee} = \frac{iE_0}{2\hbar}[\sigma_{ge}d_{eg}\sum_{n=-\infty}^{n=\infty} J_n(\kappa)(e^{-i\omega t(n-2)} + e^{-in\omega t}) \quad (30)$$

$$- \sigma_{eg}d_{ge}\sum_{n=-\infty}^{n=\infty} J_n(\kappa)(e^{in\omega t} + e^{i\omega t(n-2)})] \quad (31)$$

$$\dot{\sigma}_{eg} = -\frac{iE_0}{2\hbar}d_{eg}(\rho_{ee} - \rho_{gg})\sum_{n=-\infty}^{n=\infty} J_n(\kappa)(e^{-in\omega t} + e^{-i\omega t(n-2)}) \quad (32)$$

$$\dot{\sigma}_{ge} = \frac{iE_0}{2\hbar}d_{ge}(\rho_{gg} - \rho_{ee})\sum_{n=-\infty}^{n=\infty} J_n(\kappa)(e^{in\omega t} + e^{i\omega t(n-2)}) \quad (33)$$

$$\dot{\rho}_{gg} = \frac{iE_0}{2\hbar}[\sigma_{eg}d_{ge}\sum_{n=-\infty}^{n=\infty} J_n(\kappa)(e^{i\omega t(n-2)} + e^{in\omega t}) \quad (34)$$

$$- \sigma_{ge}d_{eg}\sum_{n=-\infty}^{n=\infty} J_n(\kappa)(e^{-in\omega t} + e^{-i\omega t(n-2)})] \quad (35)$$

$$(36)$$

3.4 Rotating Wave Approximation (RWA)

For times larger than the period of oscillation only the non-oscillating terms in the density matrix elements will be of significance, and the rest can be neglected. The effect of this approximation is visible on Figure 2 where the blue curves show the full solution, as calculated by the qutip library in Python, and the orange curves give the results when the RWA is applied. The RWA thus leads to a smoothening of oscillatory features along the trajectory of the density matrix elements. In cases of beating, such as for the σ_{eg} element, the RWA returns the envelope of the oscillation.

When applied to the TLS (equations (30) - (36)), the RWA eliminates all terms other than n = 0 in the $\sum_{n=-\infty}^{n=\infty} J_n(\kappa)e^{\pm in\omega t}$ sums and all terms different from

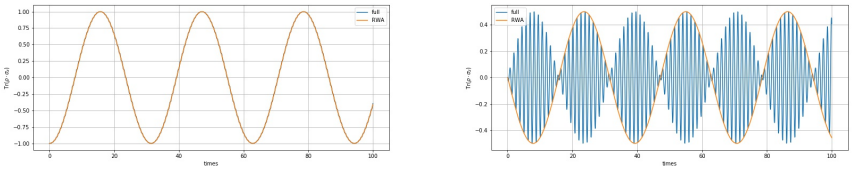

(a) ρ_{ee} (b) σ_{eg}

Figure 2: With and without RWA: Comparison of Density Matrix Elements

n = 2 in the $\sum_{n=-\infty}^{n=\infty} J_n(\kappa)e^{\pm i(n-2)\omega t}$ sums. The equations then simplify to

$$\dot{\rho}_{ee} = \frac{iE_0}{2\hbar}[(\sigma_{ge}d_{eg} - \sigma_{eg}d_{ge})(J_2(\kappa) + J_0(\kappa))] \tag{37}$$

$$\dot{\sigma}_{eg} = -\frac{iE_0}{2\hbar}d_{eg}(\rho_{ee} - \rho_{gg})(J_2(\kappa) + J_0(\kappa)) \tag{38}$$

$$\dot{\sigma}_{ge} = \frac{iE_0}{2\hbar}d_{ge}(\rho_{gg} - \rho_{ee})(J_2(\kappa) + J_0(\kappa)) \tag{39}$$

$$\dot{\rho}_{gg} = \frac{iE_0}{2\hbar}[(\sigma_{eg}d_{ge} - \sigma_{ge}d_{eg})(J_2(\kappa) + J_0(\kappa))] \tag{40}$$

Using the identity $J_2(\kappa) + J_0(\kappa) = \frac{2}{\kappa}J_1(\kappa)$:

$$\dot{\rho}_{ee} = \frac{iE_0}{\kappa\hbar}J_1(\kappa)(\sigma_{ge}d_{eg} - \sigma_{eg}d_{ge}) \tag{41}$$

$$\dot{\sigma}_{eg} = -\frac{iE_0}{\kappa\hbar}d_{eg}J_1(\kappa)(\rho_{ee} - \rho_{gg}) \tag{42}$$

$$\dot{\sigma}_{ge} = \frac{iE_0}{\kappa\hbar}d_{ge}J_1(\kappa)(\rho_{gg} - \rho_{ee}) \tag{43}$$

$$\dot{\rho}_{gg} = \frac{iE_0}{\kappa\hbar}J_1(\kappa)(\sigma_{eg}d_{ge} - \sigma_{ge}d_{eg}) \tag{44}$$

Introducing a Rabi frequency

$$\Omega_R = \frac{E_0}{\kappa\hbar}d_{eg}J_1(\kappa) = \frac{d_{eg}}{d_{ee} - d_{gg}}\omega J_1(\kappa) \tag{45}$$

transforms equations (41) - (44) to

$$\dot{\rho}_{ee} = i\Omega_R\sigma_{ge} - i\Omega_R^*\sigma_{eg} \tag{46}$$

$$\dot{\sigma}_{eg} = i\Omega_R(\rho_{gg} - \rho_{ee}) \tag{47}$$

$$\dot{\sigma}_{ge} = i\Omega_R^*(\rho_{gg} - \rho_{ee}) \tag{48}$$

$$\dot{\rho}_{gg} = i\Omega_R^*\sigma_{eg} - i\Omega_R\sigma_{ge} \tag{49}$$

where $\dot{\rho}_{ee} + \dot{\rho}_{gg} = 0$ as expected, given that the trace of the density matrix must equal 1 at all times.

Contrary to the ordinary Rabi frequency $\Omega_R = \frac{E_0 d_{eg}}{\hbar}$ for a non-polar molecule, which scales linearly with the intensity of the incident electric field, (45) produces a parabollic response as noted on Figure 1 and in the introduction.

3.5 Coupled Differential Equations and Final Solution

The next step to solving equations (46) - (49) involves the assumption that the density matrix elements take the form

$$\rho_{ee}(t) = \rho_{ee}(0)e^{\alpha t} \qquad \dot{\rho}_{ee}(t) = \alpha\rho_{ee}(0)e^{\alpha t} \tag{50}$$

$$\sigma_{eg}(t) = \sigma_{eg}(0)e^{\alpha t} \qquad \dot{\sigma}_{eg}(t) = \alpha\sigma_{eg}(0)e^{\alpha t} \tag{51}$$

$$\sigma_{ge}(t) = \sigma_{ge}(0)e^{\alpha t} \qquad \dot{\sigma}_{ge}(t) = \alpha\sigma_{ge}(0)e^{\alpha t} \tag{52}$$

$$\rho_{gg}(t) = \rho_{gg}(0)e^{\alpha t} \qquad \dot{\rho}_{gg}(t) = \alpha\rho_{gg}(0)e^{\alpha t} \tag{53}$$

where α is some constant.

Equating equations (46)-(49) to the derivatives in (50)-(53) at time t = 0:

$$\begin{pmatrix} \alpha\rho_{ee}(0) & \alpha\sigma_{eg}(0) \\ \alpha\sigma_{ge}(0) & \alpha\rho_{gg}(0) \end{pmatrix} = \begin{pmatrix} i\Omega_R\sigma_{ge}(0) - i\Omega_R^*\sigma_{eg}(0) & i\Omega_R(\rho_{gg}(0) - \rho_{ee}(0)) \\ -i\Omega_R^*(\rho_{gg}(0) - \rho_{ee}(0)) & i\Omega_R^*\sigma_{eg}(0) - i\Omega_R\sigma_{ge}(0) \end{pmatrix} \tag{54}$$

Or, in other words,

$$\begin{pmatrix} \alpha & i\Omega_R^* & -i\Omega_R & 0 \\ i\Omega_R & \alpha & 0 & -i\Omega_R \\ -i\Omega_R^* & 0 & \alpha & i\Omega_R^* \\ 0 & -i\Omega_R^* & i\Omega_R & \alpha \end{pmatrix} \begin{pmatrix} \rho_{ee}(0) \\ \sigma_{eg}(0) \\ \sigma_{ge}(0) \\ \rho_{gg}(0) \end{pmatrix} = \begin{pmatrix} 0 \\ 0 \\ 0 \\ 0 \end{pmatrix} \tag{55}$$

To have non-trivial solutions, the matrix needs to be singular:

$$det \begin{pmatrix} \alpha & i\Omega_R^* & -i\Omega_R & 0 \\ i\Omega_R & \alpha & 0 & -i\Omega_R \\ -i\Omega_R^* & 0 & \alpha & i\Omega_R^* \\ 0 & -i\Omega_R^* & i\Omega_R & \alpha \end{pmatrix} = 0 \tag{56}$$

which leads to the following values for α: $\alpha_{1,2} = 0$, $\alpha_{3,4} = \pm 2i|\Omega_R|$

The density matrix elements then take the general form

$$\rho_{ee}(t) = C_1 + C_2 e^{i2|\Omega_R|t} + C_3 e^{-i2|\Omega_R|t} \tag{57}$$

$$\sigma_{eg}(t) = D_1 + D_2 e^{i2|\Omega_R|t} + D_3 e^{-i2|\Omega_R|t} \tag{58}$$

with C_i, D_i: constants. It is sufficient to find only two elements as the others will follow from the properties of density matrices.

Setting the system to be fully in the ground state at t=0, the following initial conditions can be used

$$\rho_{ee}(0) = 0 \tag{59}$$
$$\rho_{eg}(0) = 0 \tag{60}$$
$$\rho_{ge}(0) = 0 \tag{61}$$
$$\rho_{gg}(0) = 1 \tag{62}$$

Applying (59) - (62) together with the conditions on the first and second derivatives of the density matrix elements (46)-(49) leads to the following solutions for C_i:

$$C_2 = C_3 = -\frac{1}{4} \tag{63}$$
$$C_1 = \frac{1}{2} \tag{64}$$

Substituting these values into expression (57) for the density matrix element ρ_{ee}:

$$\rho_{ee}(t) = \frac{1}{2} - \frac{1}{4}(e^{i2\Omega_R t} + e^{-i2\Omega_R t}) \tag{65}$$
$$= \frac{1}{2}(1 - cos(2\Omega_R t) \tag{66}$$
$$\tag{67}$$

Equation (46) and the values of D_i imposed by the initial conditions are now sufficient to determine the coherence σ_{eg}. Finally, this leads to a time evolution of the density matrix elements of the form

$$\rho_{ee} = sin^2(\frac{|\Omega_R|}{2}t) \tag{68}$$
$$\sigma_{eg} = -\frac{i}{2}sin(|\Omega_R|t) \tag{69}$$

3.6 Systems with Detuning

Since there is always some uncertainty associated with the energies of the atomic levels, Heisenberg's principle makes it possible for a transition to occur even when the laser frequency is not exactly in resonance. This situation is encompassed by a detuning constant $\delta = \omega_0 - \omega$. Instead of assuming $\delta = 0$, as in section 3.3, the term $i\omega_0\rho_{eg}$ from equation (19) has to be carried onwards to account for detuning. Then, the optical Bloch equations take the form

$$\dot{\rho_{ee}} = i\Omega_R\sigma^*_{eg} - i\Omega^*_R\sigma_{eg} \tag{70}$$
$$\dot{\sigma_{eg}} = -i\delta\sigma_{eg} + i\Omega_R(1 - 2\rho_{ee}) \tag{71}$$

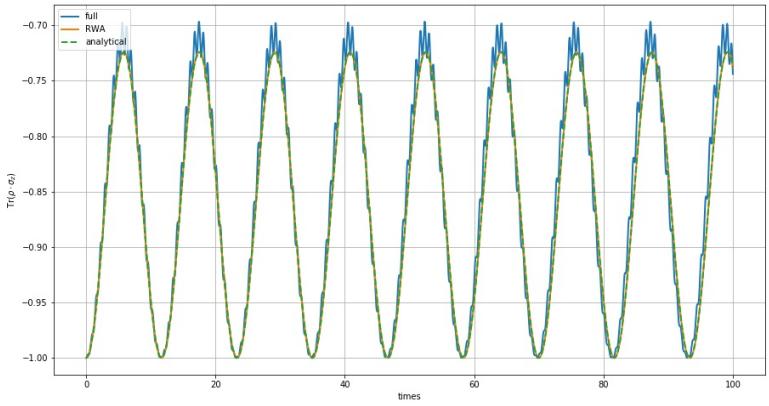

Figure 3: Oscillations of ρ_{ee} in External Field with Detuning

the only difference with equations (35) and (38) being the detuning term $-i\delta\sigma_{eg}$. These can be solved via the same method as above to give [1]

$$\rho_{ee}(t) = \frac{|\Omega_R|^2}{\Omega^2} sin^2(\Omega t) \tag{72}$$

$$\sigma_{eg}(t) = \frac{\Omega_R}{\Omega^2} sin(\Omega t)(i\Omega cos(\Omega t) - \frac{\delta}{2} sin(\Omega t)) \tag{73}$$

where $\Omega = \sqrt{\frac{\delta}{2}^2 + |\Omega_R|^2}$ is introduced to simplify expressions. When $\delta \to 0$, this expresions of course simplify to the case of light at resonance with the atomic transition (equations 68 - 69).

As shown on Figure 3, systems with detuning have a decreased probability to reach the excited state, as should be expected by the mistmatch of frequencies. The figure also serves to further illustrate some imperfections in the RWA: as time goes past, the cases where the approximation was applied get further away from the full solution. The more detuning there is in the system, the less accurate the approximation becomes.

3.7 Spontaneous Emission

Another important factor in the oscillations of a TLS is the effect of spontaneous emission. In order to account for the system's interaction with the environment, the Linbladian master equation must be used:

$$\frac{\partial\hat{\rho}}{\partial t} = -\frac{i}{h}[\hat{H}, \hat{\rho}] + \gamma(\sigma_-\rho\sigma_-^\dagger - \frac{1}{2}\{\sigma_-^\dagger\sigma_-, \rho\}) \tag{74}$$

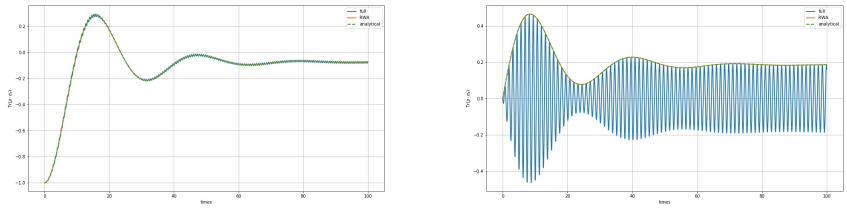

(a) ρ_{ee} (b) σ_{eg}

Figure 4: TLS with Spontaneous Emission in External Field

with $\sigma_- = \begin{pmatrix} 0 & 0 \\ 1 & 0 \end{pmatrix}$, one of the associated Pauli matrices. In the absence of spontaneous emission ($\gamma = 0$), this equation reduces to the already familiar von Neumann equation.

Starting from equation (74), and following the same procedure as outlined above, the time evolution of the density matrix elements when spontaneous emission is taken into account is found to be

$$\rho_{ee}(t) = \frac{\frac{1}{2}|\Omega_R|^2}{2(\frac{\gamma}{2})^2 + |\Omega_R|^2}[1 - (cos(\Gamma t) + \frac{3\gamma}{4\Gamma} sin(\Gamma t))]e^{-\frac{3}{4}\gamma t} \tag{75}$$

$$\sigma_{eg}(t) = \frac{i\Omega_R(\frac{\gamma}{2})}{2(\frac{\gamma}{2})^2 + |\Omega_R|^2}[1 - (cos(\Gamma t) + \frac{(\frac{\gamma}{2})^2 - |\Omega_R|^2}{\gamma\Gamma} sin(\Gamma t)]e^{-\frac{3}{4}\gamma t} \tag{76}$$

where $\Gamma = \sqrt{|\Omega_R|^2 - (\frac{\gamma}{4})^2}$ and the Rabi frequency is now again defined as $\Omega_R = \frac{d_{eg}}{d_{ee} - d_{gg}} \omega J_1(\kappa)$ as previously.

The evolution of the density matrix elements of a TLS at resonance under an external field with amplitude $E_0 = 0.2$ and experiencing spontaneous emission with a factor of $\gamma = 0.08$ is plotted on Figure 4. As expected, the amplitude of the oscillations decreases over time due to the spontaneous emission to the environment. The effect of the RWA is once again negligible as there is no detuning in the system.

Unfortunately, it is not possible to derive an analytical solution that incorporates both spontaneous emission and detuning.[1] From here onwards the atom will be assumed to be at resonance and equations (62-63) will be used. Luckily, in this scenario the effects of the RWA used in the analytical derivation are also minimized.

4 Mie Scattering by a Spherical Nanoparticle

Refractive index values of gold and silver at different wavelengths are taken from [3]

The scattering of light by spherical particles is described by the Mie solution to Maxwell's equations, which can take a variety of forms depending on the exact sum of vector harmonics. In cases where the particle is of size comparable to the wavelength of the external field, the sphere starts to act like an antenna, enhancing the electric field intensity at two opposite poles (called 'hotspots'). Therefore, a small spherical nanoparticle is proposed as a way to obtain stronger fields at two such regions in space, where an array TLS can be positioned.

The Mie scattering formalism establishes that the electric field scattered by a sphere takes the form

$$\vec{E_s} = \sum_{n=1}^{n=\infty} E_n(ia_n\vec{N}_{emn}(k,\vec{r}) - b_n\vec{M}_{omn}(k,\vec{r})) \tag{77}$$

where $E_n = \frac{i^n E_0(2n+1)}{n(n+1)}$ and $N^{(3)}_{eln}(k,\vec{r})$, $M^{(3)}_{oln}(k,\vec{r})$ are the spherical electric and magnetic vector harmonics. The amplitude of the magnetic field $|B| = \frac{|E|}{c}$ is much smaller than that of the electric field, and interactions with the magnetic component of light can safely be neglected in favor of the stronger coupling to the electric field. Furthermore, higher electric terms also get smaller, and it is sufficient to take into account only the electric dipole ($n = 1$). This approximation is justified by the plots of the scattering cross sections of silver and gold nanoparticles of radius 40 nm (Figure 5). The orange curves depend solely on the electric dipole and the blue lines take into account further electric terms, as well as magnetic terms. The magnetic dipole term, which is the strongest of the magnetic contributions is given green. It is easy to see that its effect is negligible for all wavelengths, including the resonance one, which is of most relevance to the project. The plot shows an almost perfect match between the electric dipole approximation and the curve involving more terms.

Neglecting the magnetic term simplifies equation (77) to

$$\vec{E_s} \approx \sum_{n=1}^{n=\infty} E_n(ia_n\vec{N}_{emn}(k,\vec{r})) \tag{78}$$

and removing higher order electric terms collapses the sum to

$$\vec{E_s} \approx E_1(ia_1\vec{N}_{e11}(k,\vec{r})) \tag{79}$$

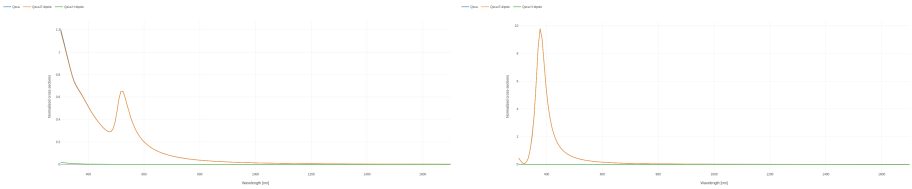

(a) ρ_{ee} (b) σ_{eg}

Figure 5: Scattering Cross Sections of Spherical Nanoparticles. *Plots produced by the Mie Scattering Calculator developed at iTMO.[4]*

where the electric spherical harmonic is given by

$$\vec{N}_{e11}(k,\vec{r}) = 2\frac{z_1(\rho)}{\rho}cos(\phi)P_1^1(cos(\theta))\vec{e_r} \tag{80}$$

$$+ cos(\phi)\frac{dP_1^1(cos(\theta))}{d\theta}\frac{1}{\rho}\frac{d}{d\rho}[\rho z_1(\rho)]\vec{e_\theta} \tag{81}$$

$$- sin(\phi)\frac{P_1^1(cos(\theta))}{sin(\theta)}\frac{1}{\rho}\frac{d}{d\rho}[\rho z_1(\rho)]\vec{e_\phi} \tag{82}$$

with $\rho = kr$, k being the wavenumber, and (r,θ,ϕ): the three spherical coordinates.

The associated Legendre polynomial $P_1^1(cos(\theta)) = -sin(\theta)$ which further simplifies the harmonic to

$$\vec{N}_{e11}(k,\vec{r}) = -2\frac{z_1(\rho)}{\rho}cos(\phi)sin(\theta)\vec{e_r} \tag{83}$$

$$- cos(\phi)cos(\theta)\frac{1}{\rho}\frac{d}{d\rho}[\rho z_1(\rho)]\vec{e_\theta} \tag{84}$$

$$+ sin(\phi)\frac{1}{\rho}\frac{d}{d\rho}[\rho z_1(\rho)]\vec{e_\phi} \tag{85}$$

with $z_1(\rho)$ a spherical Hankel function of the first kind:

$$z_1(\rho) = h_1^{(1)}(\rho) = \sqrt{\frac{\pi}{2\rho}}(J_{3/2}(\rho) + iY_{3/2}(\rho)) = \sqrt{\frac{\pi}{2\rho}}H_{3/2}^{(1)}(\rho) \tag{86}$$

where $J_{3/2}(\rho)$ and $Y_{3/2}(\rho)$ are Bessel functions of the first and second kind, respectively.

Then

$$\frac{d}{d\rho}(\rho z_1(\rho)) = \frac{d}{d\rho}\sqrt{\frac{\pi\rho}{2}}H_{3/2}^{(1)}(\rho) \tag{87}$$

$$= \sqrt{\frac{\pi\rho}{2}}(H_{1/2}^{(1)}(\rho) - \frac{H_{3/2}^{(1)}(\rho)}{\rho}) \tag{88}$$

which can be substituted in (83) - (85) to give

$$\vec{N}_{e11}(k,\vec{r}) = \sqrt{\frac{\pi}{2\rho}}[-2cos(\phi)sin(\theta)\frac{H^{(1)}_{3/2}(\rho)}{\rho}\vec{e_r} \tag{89}$$

$$- cos(\phi)cos(\theta)(H^{(1)}_{1/2}(\rho) - \frac{H^{(1)}_{3/2}(\rho)}{\rho})\vec{e_\theta} \tag{90}$$

$$+ sin(\phi)(H^{(1)}_{1/2}(\rho) - \frac{H^{(1)}_{3/2}(\rho)}{\rho})\vec{e_\phi}] \tag{91}$$

Equation (79) for the scattered field then becomes

$$\vec{E_s} \approx E_1 i a_1 \sqrt{\frac{\pi}{2\rho}}[-2cos(\phi)sin(\theta)\frac{H^{(1)}_{3/2}(\rho)}{\rho}\vec{e_r} \tag{92}$$

$$- cos(\phi)cos(\theta)(H^{(1)}_{1/2}(\rho) - \frac{H^{(1)}_{3/2}(\rho)}{\rho})\vec{e_\theta} \tag{93}$$

$$+ sin(\phi)(H^{(1)}_{1/2}(\rho) - \frac{H^{(1)}_{3/2}(\rho)}{\rho})\vec{e_\phi}] \tag{94}$$

from which the three components of the field can be easily extracted:

$$E_r = -i\sqrt{\frac{2\pi}{\rho}}E_1 a_1 cos(\phi)sin(\theta)\frac{H^{(1)}_{3/2}(\rho)}{\rho} \tag{95}$$

$$E_\theta = -i\sqrt{\frac{\pi}{2\rho}}E_1 a_1 cos(\phi)cos(\theta)(H^{(1)}_{1/2}(\rho) - \frac{H^{(1)}_{3/2}(\rho)}{\rho}) \tag{96}$$

$$E_\phi = i\sqrt{\frac{\pi}{2\rho}}E_1 a_1 sin(\phi)(H^{(1)}_{1/2}(\rho) - \frac{H^{(1)}_{3/2}(\rho)}{\rho}) \tag{97}$$

Substituting $E_1 = \frac{3}{2}iE_0$, and normalizing with respect to E_0:

$$\frac{E_r}{E_0} = 3\sqrt{\frac{\pi}{2\rho}}a_1 cos(\phi)sin(\theta)\frac{H^{(1)}_{3/2}(\rho)}{\rho} \tag{98}$$

$$\frac{E_\theta}{E_0} = \frac{3}{2}\sqrt{\frac{\pi}{2\rho}}a_1 cos(\phi)cos(\theta)(H^{(1)}_{1/2}(\rho) - \frac{H^{(1)}_{3/2}(\rho)}{\rho}) \tag{99}$$

$$\frac{E_\phi}{E_0} = -\frac{3}{2}\sqrt{\frac{\pi}{2\rho}}a_1 sin(\phi)(H^{(1)}_{1/2}(\rho) - \frac{H^{(1)}_{3/2}(\rho)}{\rho}) \tag{100}$$

Or

$$\frac{E_r}{E_0} = 3\sqrt{\frac{\pi}{2\rho}}a_1 cos(\phi)sin(\theta)(\frac{J_{3/2}(\rho)+iY_{3/2}(\rho)}{\rho}) \tag{101}$$

$$\frac{E_\theta}{E_0} = \frac{3}{2}\sqrt{\frac{\pi}{2\rho}}a_1 cos(\phi)cos(\theta)(\frac{J_{1/2}(\rho)+iY_{1/2}(\rho)}{\rho} - \frac{J_{3/2}(\rho)+iY_{3/2}(\rho)}{\rho}) \tag{102}$$

$$\frac{E_\phi}{E_0} = -\frac{3}{2}\sqrt{\frac{\pi}{2\rho}}a_1 sin(\phi)(\frac{J_{1/2}(\rho)+iY_{1/2}(\rho)}{\rho} - \frac{J_{3/2}(\rho)+iY_{3/2}(\rho)}{\rho}) \tag{103}$$

in terms $J(\rho)$ and $Y(\rho)$, the Bessel functions of the first and second kind, respectively.

In principle, given a_1, (101)-(103) are already sufficient to determine the scattered field. However, it would be easier to input points for the locations of the TLS in Cartesian coordinates.

The spherical basis vectors transform into Cartesian coordinates as

$$\vec{e_r} = sin(\theta)cos(\phi)\vec{e_x} + sin(\theta)sin(\phi)\vec{e_y} + cos(\theta)\vec{e_z} \tag{104}$$

$$\vec{e_\theta} = cos(\theta)cos(\phi)\vec{e_x} + cos(\theta)sin(\phi)\vec{e_y} - sin(\theta)\vec{e_z} \tag{105}$$

$$\vec{e_\phi} = -sin(\phi)\vec{e_x} + cos(\phi)\vec{e_y} \tag{106}$$

Therefore

$$\vec{E_s} = (E_r sin(\theta)cos(\phi) + E_\theta cos(\theta)cos(\phi) - E_\phi sin(\phi))\vec{e_x} \tag{107}$$

$$+ (E_r sin(\theta)sin(\phi) + E_\theta cos(\theta)sin(\phi) + E_\phi cos(\phi))\vec{e_y} \tag{108}$$

$$+ (E_r cos(\theta) - E_\theta sin(\theta))\vec{e_z} \tag{109}$$

or in component form:

$$\frac{E_x}{E_0} = (\frac{E_r}{E_0}sin(\theta)cos(\phi) + \frac{E_\theta}{E_0}cos(\theta)cos(\phi) - \frac{E_\phi}{E_0}sin(\phi)) \tag{110}$$

$$\frac{E_y}{E_0} = (\frac{E_r}{E_0}sin(\theta)sin(\phi) + \frac{E_\theta}{E_0}cos(\theta)sin(\phi) + \frac{E_\phi}{c}os(\phi)) \tag{111}$$

$$\frac{E_z}{E_0} = (\frac{E_r}{E_0}cos(\theta) - \frac{E_\theta}{E_0}sin(\theta)) \tag{112}$$

with the coordinate transformations given in the usual way:

$$\rho = kr = k\sqrt{x^2+y^2+z^2} \tag{113}$$

$$\theta = arctan(\frac{\sqrt{x^2+y^2}}{z}) \tag{114}$$

$$\phi = arctan(\frac{y}{x}) \tag{115}$$

For any point (x,y,z), transforming into spherical coordinates via (113) - (115), then computing the normalized spherical components of the field via (101) - (103) and plugging them into (110) - (112) allows to obtain the normalised Cartesian components of the field which will be relevant for calculating the Rabi frequency of the atomic transitions. This approach is easily programmable as it allows for the calculation of the field to be broken off into three smaller functions, much in the same way as it was presented throughout this section. The results of such simulations will be discussed in detail in sections 4.2 and 4.3, but for now, there is one more element that still needs to be determined: the scattering coefficient a_1.

4.1 Scattering Coefficients: The Mystical a_1

Since there appeared to be some ambiguity in the notation for Mie scattering coefficients in different sources (for example [5] and [6]), four separate derivations were compared graphically and found to give the same results up to an exchange of the a_n and b_n terms. In this report, the a_1 coefficient is taken to have its usual meaning of a first order *electric* scattering coefficient.

Taken without proof from Mie theory, the a_n terms have the form

$$a_n = \frac{\Psi'_n(y)\Psi_n(x) - m\Psi_n(y)\Psi'_n(x)}{\Psi'_n(y)\Xi_n(x) - m\Psi_n(y)\Xi'_n(x)} \tag{116}$$

where $x = ka$, $y = mka$, with a being the radius of the particle, and m: its refractive index. [6]

The functions Ψ and Ξ are Ricatti-Bessel spherical functions which take the form:

$$\Psi_n(z) = zj_n(z) \tag{117}$$

$$\Xi_n(z) = zh_n^{(2)}(z) \tag{118}$$

with $j_n(z)$ and $h_n^{(2)}$, a spherical Bessel function of the nth order, and a spherical Hankel function of the nth order and second kind, respectively. These can be rewritten in terms of Bessel functions:

$$\Psi_n(z) = \sqrt{\frac{\pi z}{2}} J_{n+1/2}(z) \tag{119}$$

$$\Xi_n(z) = \sqrt{\frac{\pi z}{2}} (J_{n+1/2}(z) - iY_{n+1/2}(z)) \tag{120}$$

Taking the first derivatives:

$$\Psi'_n(z) = \sqrt{\frac{\pi z}{2}} (J_{n-1/2}(z) - \frac{n}{z}) J_{n+1/2}(z) \tag{121}$$

$$\Xi'_n(z) = \sqrt{\frac{\pi z}{2}} (J_{n-1/2}(z) - iY_{n-1/2}(z) - \frac{n}{z}(J_{n+1/2}(z) - iY_{n+1/2}(z)) \tag{122}$$

For any given input wavelength, refractive index and radius of the nanoparticle, the variables x and y xan be readily substituted into expressions (119) - (122) which can be used to calculated the a_n coefficient (116). This method is again very easy to break down into separate functions and thus simple to program. As already discussed, only the a_1 coefficient is of relevance to the project, but higher order terms and magnetic coefficients [6] are also given for completion in order to further test the assumption that they play little role in the Mie scattering by small spheres:

$$b_n = \frac{m\Psi'_n(y)\Psi_n(x) - \Psi_n(y)\Psi'_n(x)}{m\Psi'_n(y)\Xi_n(x) - \Psi_n(y)\Xi'_n(x)} \tag{123}$$

4.2 Scattering, Extinction and Absorption Cross Sections

Using the Mie scattering coefficients, three useful quantities can be defined: the scattering, extinction and absorption cross sections that give respectively the amount of light scattered by, incident on, and absorbed by the particle. [7], [6]

$$Q_{sca} = \frac{\lambda^2}{2\pi} \sum_{n=0}^{n=\infty} (2n+1)(|a_n|^2 + |b_n|^2) \tag{124}$$

$$Q_{ext} = \frac{\lambda^2}{2\pi} \sum_{n=0}^{n=\infty} (2n+1) Re(a_n + b_n) \tag{125}$$

$$Q_{abs} = Q_{ext} - Q_{sca} \tag{126}$$

Taking into account only the $n = 1$ terms:

$$Q_{sca} = \frac{3\lambda^2}{2\pi}(|a_1|^2 + |b_1|^2) \tag{127}$$

$$Q_{ext} = \frac{3\lambda^2}{2\pi} Re(a_1 + b_1) \tag{128}$$

$$Q_{abs} = Q_{ext} - Q_{sca} \tag{129}$$

These cross sections are plotted on Figures 6-8, with black circles taking the solution from iTMO [4] that contains many terms (higher n-coefficients), the purple squares signifying solutions with just the dipole terms (a_1 and b_1) taken into account, and the blue crosses incorporating only the electric dipole term a_1 ($b_1 = 0$). The wavelengths and corresponding refractive indices come from McPeak's data on gold nanoparticles. [3]

As can be seen on all three figures, the electric dipole term gives a very good match to the full solution near the resonance peak, and at wavelengths higher than that, so it is justified to keep only the a_1 coefficient in Mie scattering expressions.

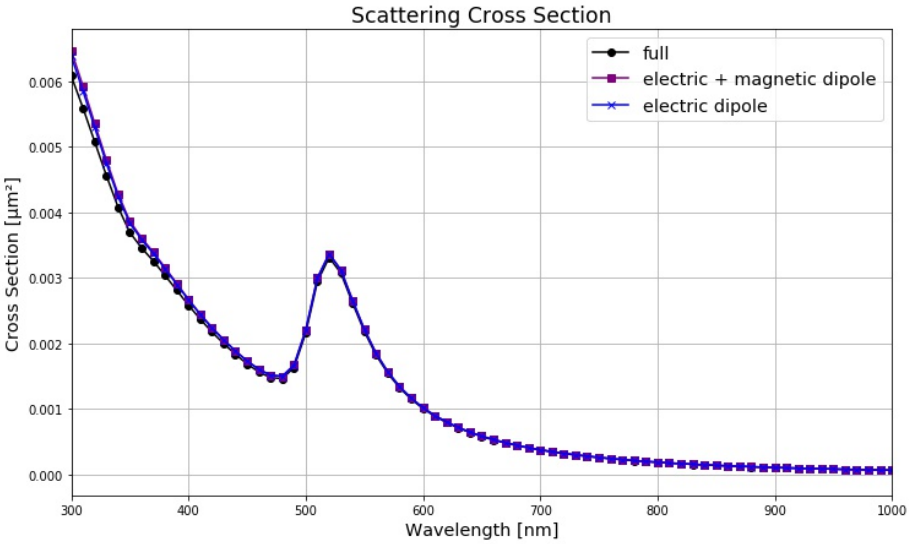

Figure 6: Validity of approximations: scattering cross section

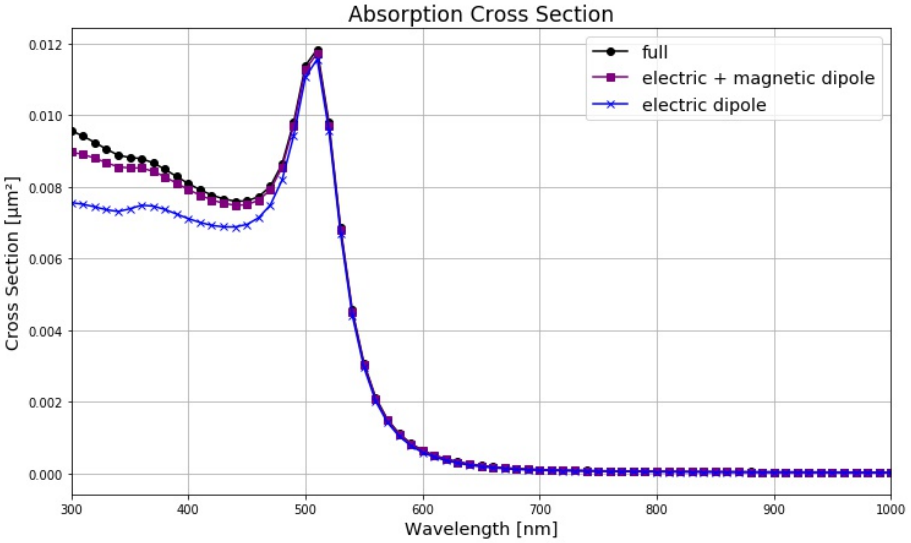

Figure 7: Validity of approximations: absorption cross section

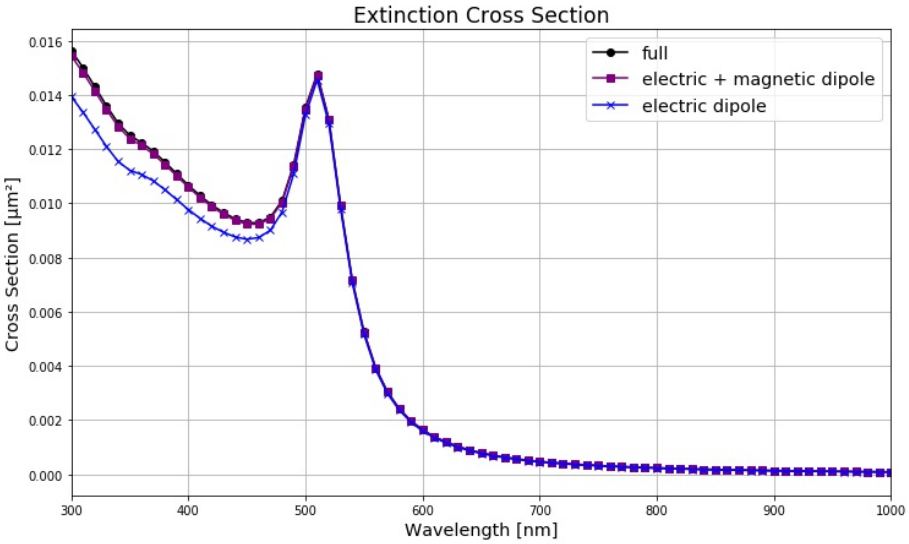

Figure 8: Validity of approximations: extinction cross section

Finally, Figure 9 presents a harsh trade-off of variables: although scattering peaks at the resonance wavelength, so does absorption. Therefore, a higher scattered intensity might actually be achieved by using light that is of a wavelength slightly higher than the resonance: in this way less photons will be absorbed by the nanoparticle and more of the light will be emitted. Such scenarios are not considered in this report but the supporting jupyter notebooks could be used to investigate Mie scattering at any wavelength, as long as the dipole approximation holds true.

4.3 Scattered Field Components

Now that a_1 has been defined, the procedure outlined in the section above can be used to find the Cartesian components of the scattered field. One example of these component values is presented on Figure 10. Since light travels in the $\hat{z}$ direction, there is very little light scattered along the z-axis, as the particle blocks it off almost completely. The polarisation of the incident field is in the $\hat{x}$ direction, which matches with the plot where the highest scattering of light is observed along x-axis. Although this cannot be seen on the plot on Figure 10, the amplitude of the E_x component is indeed found to be larger than that of E_y. Finally, we should note that there is no E_y component at $x = 0$, while the E_x component there is at its maximum. Thus, positioning the array of TLS along a vertical line passing through $x = 0$ would ensure that they are placed in a gradient of an intense electric field of amplitude E_x that is fully x-polarised, thus keeping in line with our assumptions about the direction of the PDMs of the TLSs.

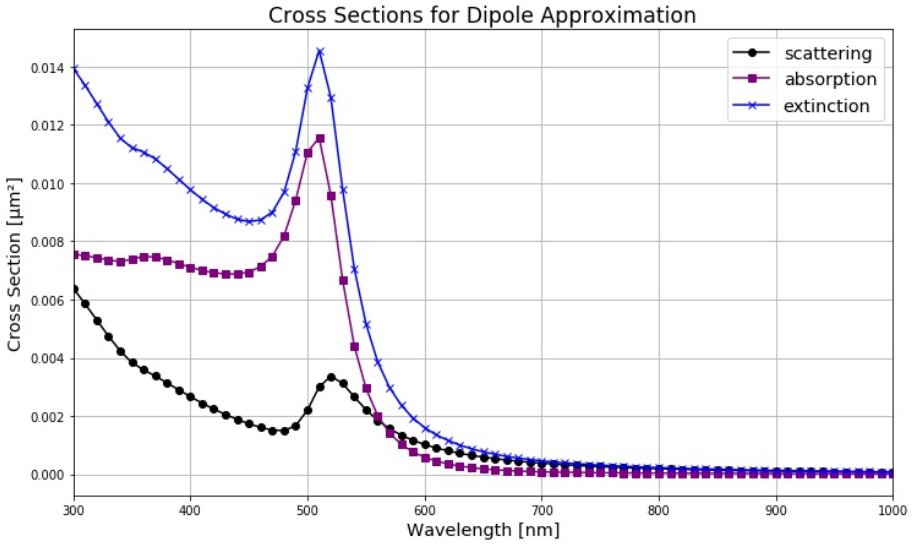

Figure 9: Trade-off of variables

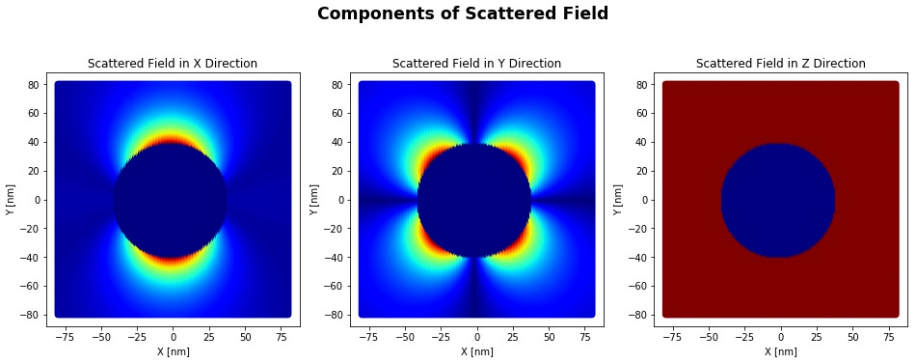

Figure 10: Components of scattered field for gold nanoparticle of radius $a = 40$ nm at $z = 0$ under light of wavelength 540 nm

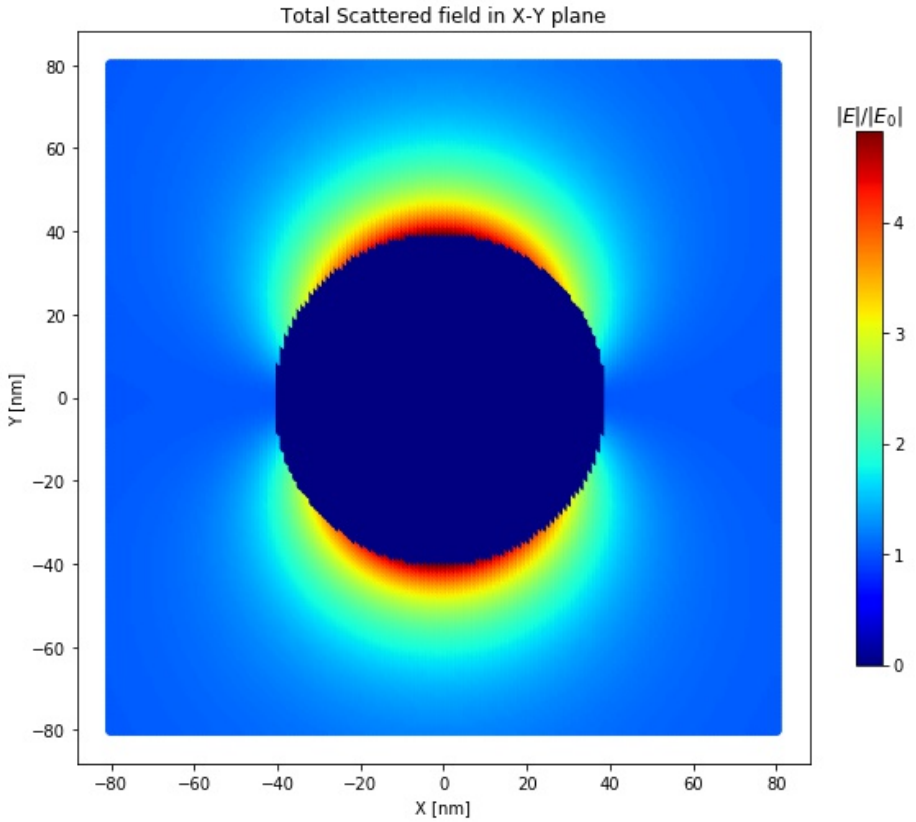

Figure 11: Field scattered by a gold nanoparticle of radius $a = 40$ nm under light of wavelength 520 nm

4.4 Scattered Field for Gold and Silver Nanoparticles

Finally, the algorithm for finding field components enables a calculation of the full scattered field. Figures 11 and 12 show the $z = 0$ cross-sections of the field for gold and silver nanoparticles, respectively, each of radius $a = 40$ nm and illuminated by light of wavelength 540 nm. An important point to note is that the scattered field is renormalised to $\frac{|E_0+E_s|}{|E_0|}$ to allow a comparison with iTMO simulations [4] which follow this convention.

While both nanoparticles lead to a strong enhancement of the light, silver appears to be a better candidate for the project as it leads to a scattered field at the two hotspots that is more than twice stronger. This is due to the lower resonance wavelength of silver, which corresponds to a lower real part n, and a higher imaginary part k of the refractive index m.

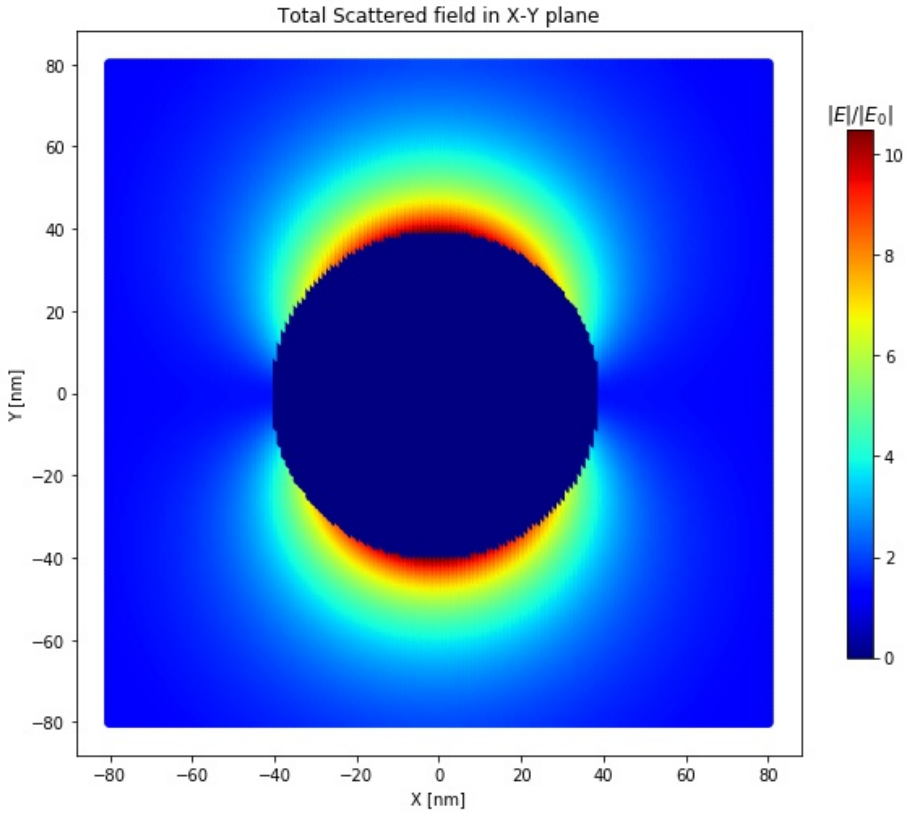

Figure 12: Field scattered by a silver nanoparticle of radius $a = 40$ nm under light of wavelength 520 nm

5 Bringing it together: Evolution of TLS in the Vicinity of a Nanoparticle

Sections 3 and 4 provide the necessary machinery to solve for the oscillation of a TLS positioned at the hotspot of a nanoparticle with some set parameters of the particle, the surrounding environment, and the value for the initial field. In order to combine these two segments of the project, one would have to proceed backwards through the report: first, calculating the value of the scattered field at the set coordinates, and then finding the time evolution that a TLS will experience if placed under a field of such intensity. Extending this to more than one TLS should be elementary: one would just need to repeat the same process all over again for the full array of coordinates of the atoms. As with many things in life however, what appeared to be an easy problem turned out to be quite the ordeal.

5.1 Gamma Factors of Spontaneous Emission

As it happens to be, this report has now outlined all but one of the necessary ingredients for solving the problem at hand. The missing piece is the gamma factor which describes the rate of spontaneous emission. As a property arising from the contact of the TLS with its surroundings, spontaneous emission is solely affected by the parameters of the external field.

The factor γ that represents this process is described in literature as a set of two values: a normal and a tangential component ($\gamma_\perp$ and $\gamma_\parallel$, respectively). Given that the TLS are to be placed along the x-axis, and oriented parallel to it, the relevant rate of spontaneous emission would be $\gamma_\perp$, the component perpendicular to the surface of the nanosphere.

In addition, two different modes of the gamma factor could be considered: a radiative one for cases where energy is emitted in the form of light, and a non-radiative one that corresponds to the emission of heat. In this project, the dominant rate of spontaneous emission is the non-radiative one, as the energy difference between the two atomic levels is small.

As illustrated by Young et al.,[8] the normalised non-radiative rates of spontaneous emission are described by the following equations:

$$\frac{\gamma_\perp}{\gamma_0} = 1 + \frac{3}{2} Re \sum_{n=1}^{n=\infty} (2n+1) n(n+1) a_n [\frac{h_n^{(1)}(\rho)}{\rho}]^2 \tag{130}$$

$$\frac{\gamma_\parallel}{\gamma_0} = 1 + \frac{3}{2} Re \sum_{n=1}^{n=\infty} (n+\frac{1}{2}) (a_n [\frac{\Xi_n'(\rho)}{\rho}]^2 + b_n [h_n^{(1)}(\rho]^2) \tag{131}$$

And the normalised radiative rates [8] are given by

$$\frac{\gamma_{\perp}^{R}}{\gamma_0} = \frac{3}{2}\sum_{n=1}^{n=\infty} n(n+1)(2n+1)|\frac{j_n(\rho) + a_n h_n^{(1)}(\rho)}{\rho}|^2 \tag{132}$$

$$\frac{\gamma_{\parallel}^{R}}{\gamma_0} = \frac{3}{4}\sum_{n=1}^{n=\infty} (2n+1)(|j_n(\rho) + b_n h_n^{(1)}|^2 + |\frac{\Psi_n^{'}(\rho) + a_n \Xi_n^{'}(\rho)}{\rho}|^2) \tag{133}$$

Although the electric dipole approximation is still applicable, and the a_1 coefficient is greater than any other term from the Mie scattering expansion, it is no longer viable to neglect higher order electric and magnetic terms. The reason for this is that expressions (130) - (133) include Bessel and Hankel functions as part of the sums over n. When approximated to just one term, these functions result in gamma coefficients that bend away from the $\gamma = 1$ line at large distances from the particle, which is unphysical. However, it was discovered that $n = 4$ terms are sufficient to mimic the expected behaviour (γ converging towards 1) away from the nanoparticle.

The computational results with the $n = 4$ approximation were compared against a plot from Young, et al.'s paper [8] with set parameters: incident wavelength $\lambda = 4133$ nm, radius of the nanoparticle $a = 10$ nm, refractive index $m = -4.42 + 0.73i$. Data from the paper is displayed on Figure 13 alongside computational results of the current project, and it can easily be seen that there is a very satisfactory match between the two plots. This confirms that it is sufficient to take into account $n = 4$ terms in gamma factor expressions.

Another important feature of the plots on Figure 13 is that the solid lines on (a) represent the total (radiative + non-radiative) emission while the solid lines on (b) show only the non-radiative terms. The two match almost perfectly, showing that the non-radiative emission is indeed the dominant mode.

5.2 The Bad News About Gamma Factors

Despite the agreement with theory signified by Figure 13, the calculated gamma factors for other input parameters often take unphysical values. Figure 14 shows a plot for $\lambda = 540$ nm, $a = 40$ nm, $m = 0.37250206 - 2.45166429i$ i.e. gold at near resonance.[3] Two of the four gamma factor components are clearly nonsensical as they take negative values. What makes it even worse, is that one of them is exactly the normal non-radiative component that is most important for the project. Although the values seem to become positive for larger distances from the particle that is not really of relevance: the purpose of the nanoparticles in the project is field enhancement, which is always stronger nearer the particle. Similar, and equally unsatisfying results, are plotted for silver on Figure 15. Both plots utilize exactly the same functions as those used to produce Figure 13 (b).

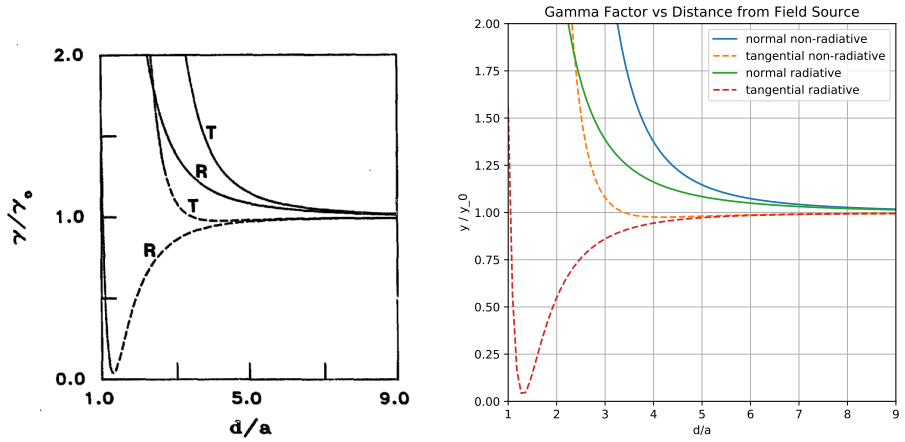

(a) Results from [8], Fig.1. R: radiative, T: total

(b) Computational results with $n = 4$ terms

Figure 13: Comparison with literature of gamma factor values for $\lambda = 4133$ nm, $a = 10$ nm, $m = -4.42 + 0.73i$

There is a number of possibilities for the underperformance of the algorithm at conditions different from the ones tested by the Young et al. paper:

1. The computational algorithm used in the project deviates from the theoretical model presented in equations (130) - (133) by the number of terms ($n = 4$) taken into account. This approximation works fine for the conditions set out on Figure 13, but is not acceptable for the gold and silver nanoparticles on Figures 14 and 15.

2. There is a mistake in the computational algorithm used that is not exhibited when testing for the conditions on Figure 13, but becomes important otherwise.

3. The theoretical model developed in Young et al. is not accurate.

The possible steps to test which item of this list is correct and to solve the problem of negative gamma factors go as follows:

1. Increase the number of n terms. When n was set to 20, the gamma factor started diverging more sharply towards the negative limit.

2. Check that the functions match the equations given in the paper. The correct results on Figure 13 seem promising, but there is always some likelihood that there are incidental.

3. Find another derivation of gamma factors in literature and use that to derrive an analytical solution. Alternatively, find sources that can give

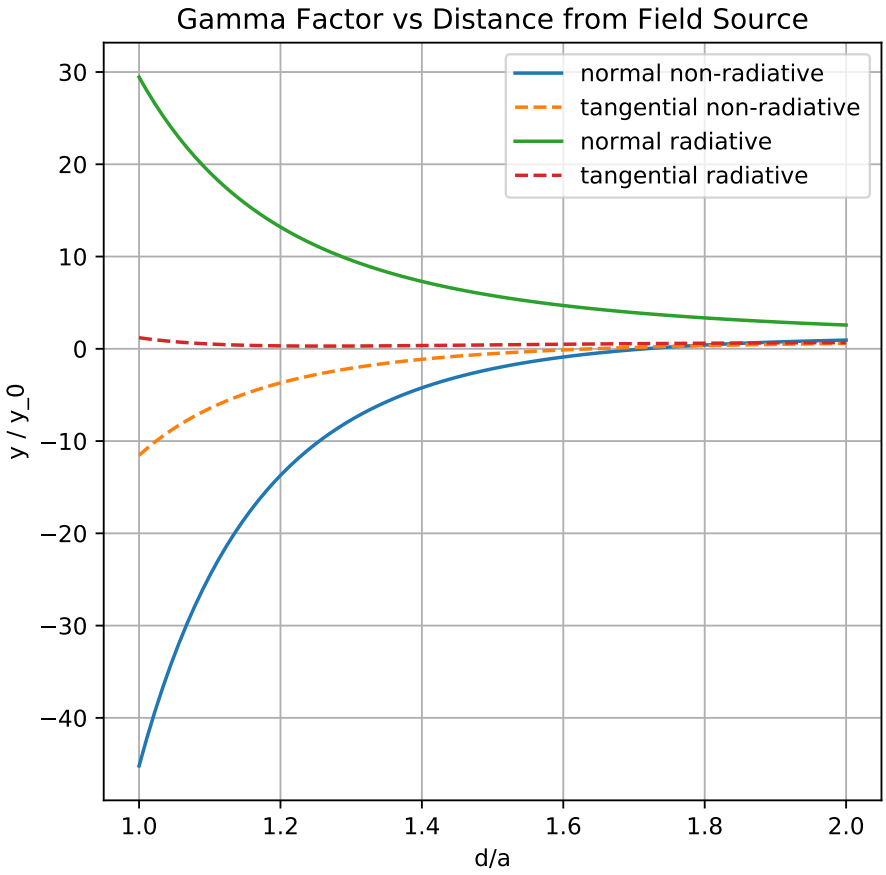

Figure 14: Gamma Factors for Gold Nanoparticle: $\lambda = 540$ nm, $a = 40$ nm, $m = 0.37250206 - 2.45166429i$

exact values of the rate of spontaneous emission for the given input parameters.

Scenarios 2. and 3. seem to be most promising, however a solution has unfortunately not been ruled out yet due to the time restrictions of the project.

5.3 Beyond the Gamma Factor Struggle

Without appropriate rates of spontaneous emission to account for the gradient of electric field values which different TLS are to experience, the connection of Sections 3 and 4 of this report remains incomplete (In fact, incorporating negative gamma factors in the density matrix evolution (75)-(76) would lead to the amplitude of oscillations increasing over time, which is non-physical). However, the required Python functions for merging the time evolution of the

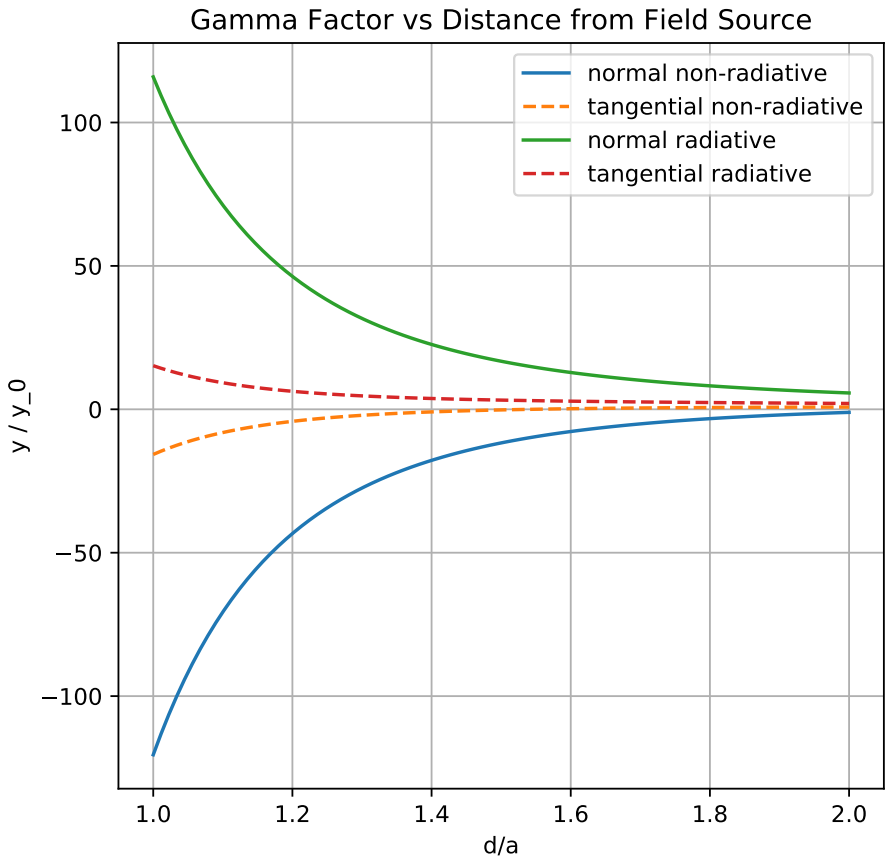

Figure 15: Gamma Factors for Silver Nanoparticle: $\lambda = 380$ nm, $a = 40$ nm, $m = 0.05075241 - 1.85872962i$

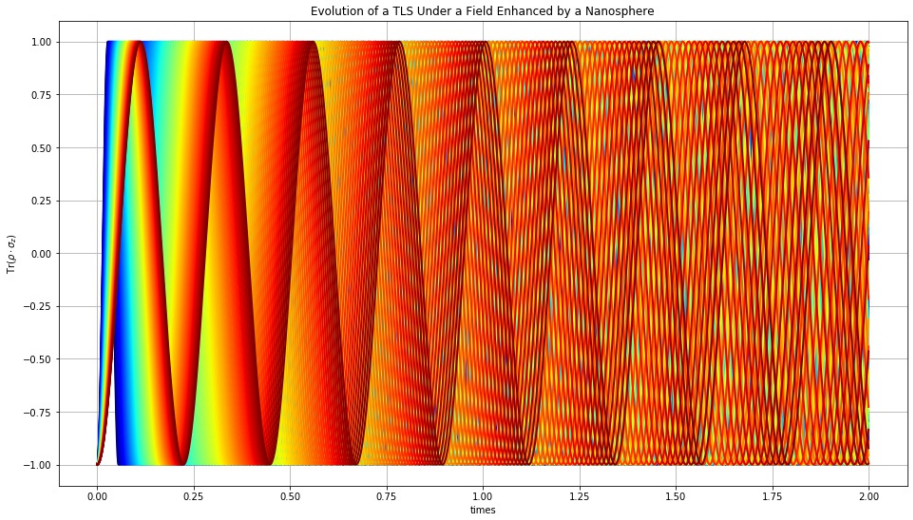

Figure 16: Evolution of Non-Polar TLS Placed at Hotspots of Silver Nanoparticle: $\lambda = 380$ nm, $a = 40$ nm, $m = 0.05075241 - 1.85872962i$, $E_0 = 10$

TLS with the field scattered by a spherical nanoparticle, are already developed. As an example of their output, Figure 16 plots the time evolution of a system of non-polar TLS at resonance with the light enhanced by the silver nanoparticle around which they are positioned in the manner described in previous sections. Each line plots the evolution of a different TLS, and as expected for a non-polar system, the lines diverge from $t = 0$ i.e. no coherent response is observed.

6 Conclusion

Although the required machinery to treat a TLS in the proximity of a light-scattering spherical nanoparticle has been developed, the project still stands unfinished until an appropriate expression for gamma factors is found. Once that problem is fixed, the machinery developed in this report should be sufficient to plot the time evolution of a series of TLS with PDM positioned at the two hotspots of the nanosphere.

References

[1] Gładysz P. Propagation of a low-frequency impulse in a medium of asymmetric atomic systems. Toruń, Poland; 2019.

[2] Blum K. Density Matrix Theory and Applications. Springer Science; 1981.

[3] McPeak KM, Jayanti SV, Kress SJP, Meyer S, Iotti S, Rossinelli A, et al. Plasmonic films can easily be better: Rules and recipes. ACS Photonics 2. 2015:326-33.

[4] Ladutenko K, Pal U, Rivera A, Peña-Rodríguez O. Mie calculation of electromagnetic near-field for a multilayered sphere. Comp Phys Comm. 2017;214:225-30.

[5] Guzatov DV, Vaschenko SV, Stankevich VV, Lunevich AY, Glukhov YF, Gaponenko SV. Plasmonic Enhancement of Molecular Fluorescence near Silver Nanoparticles: Theory, Modeling, and Experiment. J Phys Chem C. 2012;116:10723—10733.

[6] Thovsen KB. Evaluation of Mie scatter approximation formulas for the scattering of infrared light at biological cells; 2013. Available from: https://api.semanticscholar.org/CorpusID:124119456.

[7] Hahn DW. Light Scattering Theory (PDF). 2009.

[8] Kim YS, Leung PT, George TF. Classical decay rates for molecules in the presence of a spherical surface: A complete treatment. Surface Science. 1988;195(1):1-14. Available from: https://www.sciencedirect.com/science/article/pii/0039602888907765.